The application of Fresnel zone plate based projection in optofluidic microscopy

Jigang Wu*, Xiquan Cui, Lap Man Lee, and Changhuei Yang

Department of Electrical Engineering, California Institute of Technology, Pasadena, California, 91125
**Email: jigang@caltech.edu*

Abstract: Optofluidic microscopy (OFM) is a novel technique for low-cost, high-resolution on-chip microscopy imaging. In this paper we report the use of the Fresnel zone plate (FZP) based projection in OFM as a cost-effective and compact means for projecting the transmission through an OFM's aperture array onto a sensor grid. We demonstrate this approach by employing a FZP (diameter = 255 μm, focal length = 800 μm) that has been patterned onto a glass slide to project the transmission from an array of apertures (diameter = 1 μm, separation = 10 μm) onto a CMOS sensor. We are able to resolve the contributions from 44 apertures on the sensor under the illumination from a HeNe laser (wavelength = 633 nm). The imaging quality of the FZP determines the effective field-of-view (related to the number of resolvable transmissions from apertures) but not the image resolution of such an OFM system – a key distinction from conventional microscope systems. We demonstrate the capability of the integrated system by flowing the protist *Euglena gracilis* across the aperture array microfluidically and performing OFM imaging of the samples.

OCIS codes: (110.0110) Imaging Systems; (050.1970) Diffraction and gratings: Diffractive optics; (110.1220) Apertures.

References and links

1. X. Heng, D. Erickson, L. R. Baugh, Z. Yaqoob, P. W. Sternberg, D. Psaltis, and C. Yang, "Optofluidic microscopy – a method for implementing a high resolution optical microscope on an chip," Lab on a chip **6**, 1274-1276 (2006).
2. X. Cui, L. M. Lee, X. Heng, W. Zhong, P. W. Sternberg, D. Psaltis, and C. Yang, "Lensless high-resolution on-chip optofluidic microscopes for *Caenorhabditis elegans* and cell imaging," Proc. Natl. Acad. Sci. **105**, 10670-10675 (2008).
3. X. Heng, E. Hsiao, D. Psaltis, and C. Yang, "An optical tweezer actuated, nanoaperture-grid based optofluidic microscope implementation method," Opt. Express **15**, 16367-16375 (2007).
4. G. M. Whitesides, "The origins and the future of microfluidics," Nature **442**, 368-373 (2006).
5. A. G. Michette, *Optical systems for soft X rays* (Plenum Press, 1986), chapter 8.
6. W. Chao, E. Anderson, G. P. Denbeaux, B. Harteneck, J. A. Liddle, D. L. Olynick, A. L. Pearson, F. Salmassi, C. Y. Song, and D. T. Attwood, "20-nm-resolution soft x-ray microscopy demonstrated by use of multilayer test structures," Opt. Lett. **28**, 2019-2021 (2003).
7. E. Di Fabrizio, F. Romanato, M. Gentili, S. Cabrini, B. Kaulich, J. Susini, and R. Barrett, "High-efficiency multilevel zone plates for KeV X-rays," Nature **401**, 895-898 (1999).
8. R. M. Henkelman and M. J. Bronskill, "Imaging extended objects with a Fresnel-zone-plate aperture," J. Opt. Soc. Am. **64**, 134-137 (1974).
9. M. Young, "Zone plates and their aberrations," J. Opt. Soc. Am. **62**, 972-976 (1972).
10. F. Wyrowski, "Diffractive optical elements: iterative calculation of quantized, blazed phase structures," J. Opt. Soc. Am. A **7**, 961-969 (1990).
11. A. R. Jones, "The focal properties of phase zone plates," J. Phys, D: Appl. Phys. **2**, 1789-1791 (1969).
12. S. W. Hu, X. Ren, M. Bachman, C. E. Sims, G. P. Li, and N. Allbritton, "Surface modification of Poly(dimethylsiloxane) microfluidic devices by ultraviolet polymer grafting," Anal. Chem. **74**, 4117-4123 (2002).

#99006 - $15.00 USD Received 17 Jul 2008; revised 6 Sep 2008; accepted 11 Sep 2008; published 18 Sep 2008

13. X. Heng, X. Cui, D. W. Knapp, J. Wu, Z. Yaqoob, E. J. McDowell, D. Psaltis, and C. Yang, "Characterization of light collection through a subwavelength aperture from a point source," Opt. Express **14**, 10410 (2006).

1. Introduction

The optofluidic microscope (OFM) method [1-3] developed recently enables the construction of high-resolution and low-cost chip-level microscopes. Combined with the appropriate high flow-velocity microfluidic techniques [4], OFM systems can potentially address a large number of biomedical applications, such as image-based cytometry, blood parasite diagnosis and water quality inspection. The OFM imaging approach differs significantly from the conventional microscopy approach; the design choice is motivated by the fact that the conventional microscope design, with its requisite high precision optical elements, is difficult to miniaturize cost-effectively.

In its typical format, an OFM system consists of three parts: an array of apertures patterned on a metal-coated linear array sensor, a microfluidic channel emplaced on the aperture array such that the aperture array spans the channel floor in a skewed pattern, and a uniform light field projected through the microfluidic channel to the aperture array. As a sample flows through the channel and across each aperture, it interrupts light transmission through the aperture. Each transmission time trace in effect represents a line scan across the object. By ensuring that the microfluidic channel is arranged such that the separation of adjacent apertures perpendicular to the channel flow axis is smaller than the aperture diameter, we can ensure that each point on the sample is scanned [2]. By compiling all of the line scans appropriately, we can create a microscopy image of the sample in which the optimal resolution is fundamentally limited by the aperture size. This lensless design allows us to build highly compact and high-resolution microscope systems with commercially available CMOS and CCD sensor chips in a simple and cost-effective way.

While the typical OFM design calls for the aperture array to be patterned directly onto a metal-coated linear array sensor, there are certain scenarios for which a different OFM design, where the aperture array and the sensor are separated, would actually be better. Here are two of the more important scenarios: 1) Recycling/retrieval of optical sensor is desired. The typical OFM structure is not particularly easy to dismantle. If the optical sensor employed is inexpensive, this would not be an important consideration as the complete replacement of an entire expended OFM system would be more cost-effective. On the other hand, if the cost of optical sensor employed is high, an OFM design that allows easy disassembly and recovery of the optical sensor would be highly desirable. 2) Cooling of the optical sensor is desired. Operating an optical sensor at a low temperature can help reduce noise and improve signal-to-noise ratio. While cooling the OFM optical sensor to sub-freezing temperatures is easily achievable, the close proximity of the aperture array and the microfluidic channel to the optical sensor implies that that such cooling will likely freeze the microfluidic channel content as well. As such, an OFM design in which the aperture array and the microfluidic channel are well separated from the optical sensor is desirable in such a scenario.

In the paper, we report an OFM design that incorporates a Fresnel zone plate (FZP) to relay the light transmissions through the aperture array to an optical sensor. This design, termed FZP-OFM, achieves the desired separation of the aperture array and the optical sensor without compromising on the resolution of the OFM system. The FZP can be used to focus the light and form images [5-7]. However, direct imaging by FZP suffers from multiple diffractions and serious aberrations for extended objects [8, 9]. These disadvantages prevent the FZP from being widely used in imaging applications, especially in the visible regime where better conventional refractive optics is available. Nevertheless, as the FZP in our FZP-OFM design is only used to project the transmissions from the apertures onto an optical sensor, the OFM resolution (dependent on the aperture size) is unaffected by the FZP's aberration characteristics as long as the transmission projections from the apertures are

#99006 - $15.00 USD Received 17 Jul 2008; revised 6 Sep 2008; accepted 11 Sep 2008; published 18 Sep 2008

differentiable. Finally, we note that it is possible to design a general diffractive optical element (DOE) other than the FZP to increase the imaging performance in non-paraxial region [10]. However, the resulting DOE is generally more complicated and requires more efforts to design and fabricate.

As the FZP can be cost-effectively fabricated with current microfabrication techniques such as optical or electron-beam lithography, the manufacturing cost associated with this OFM design is anticipated to be low.

The following sections are structured as follows. In section 2, we show the system setup and experiment methods. In section 3, we demonstrate the capability of our system by imaging the protist *Euglena gracilis*, and the resulting images are compared with images acquired by FZP directly and conventional microscope images. Finally, we summarize our work in section 4.

2. Experiment methods

The FZP was designed to have a focal length of f = 800 μm. The radius of the m^{th} zone was calculated by [5]

$$r_m = \sqrt{m\lambda f} \tag{1}$$

where λ is the wavelength of illumination light. Our FZP has 32 zones with an outer diameter of 255 μm. The imaging scheme of the FZP is shown in Fig. 1(a). The aperture array located at 1 mm (equivalent distance in glass is 1.5 mm because of the glass refractive index of 1.5) from the FZP was imaged onto the imaging plane located at 4 mm from the FZP. The magnification (M) of the system is M = 4. The coordinate system is also shown in the figure.

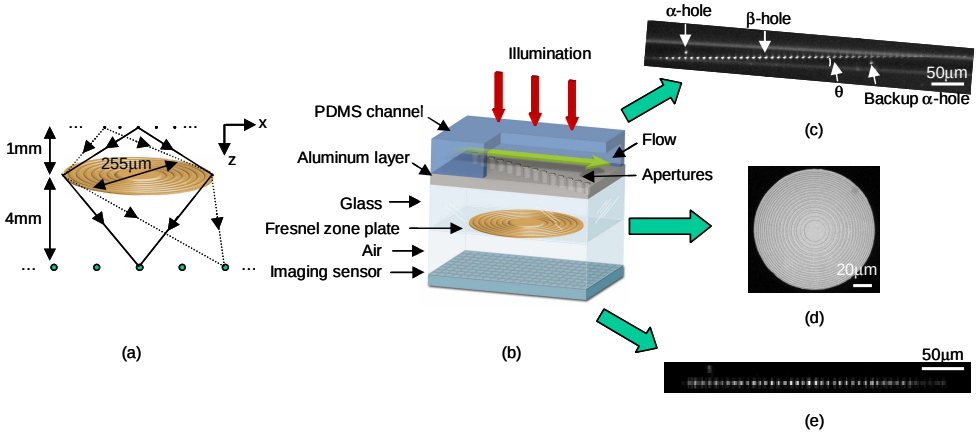

Fig. 1. (a) Imaging scheme of the FZP; (b) Illustration of the FZP-OFM system setup. (c) PDMS microchannel aligned and attached to the aluminum layer with tiny aperture array. (d) Microscope image of the fabricated FZP; (e) Image of the aperture array by the FZP.

The system setup is shown in Fig. 1(b). The system consists of two separated parts: the FZP-OFM chip with poly(dimethylsiloxane) (PDMS) microfluidic channel and an imaging sensor. To make the FZP-OFM chip, a glass wafer was coated with 300-nm-thick aluminum layer by thermal evaporator (Veeco 7760) and an array of tiny apertures (diameter = 1 μm, separation = 10 μm) was drilled by focused ion beam (FEI Nova 200). The glass wafer was then attached to another glass slide where a FZP was fabricated on the other side using photolithography (Karl Suss MJB3) with 500-nm-thick SU-8 photoresist. Finally a 200-nm-thick poly(methyl methacrylate) (PMMA) layer was spin-coated onto the aluminum layer to protect the aperture array. The PDMS microchannel (width = 25 μm, height = 16 μm) was fabricated by transferring the microfluidic structure from the prefabricated SU-8 mold to the

#99006 - $15.00 USD Received 17 Jul 2008; revised 6 Sep 2008; accepted 11 Sep 2008; published 18 Sep 2008

PDMS elastomer. Then the microchannel was aligned to the aperture array and attached to the aluminum layer of the FZP-OFM chip under microscope. The optical sensor (Lumenera Lu-080M, with 9.9-μm pixel size) was located at the imaging plane of the FZP and the aperture array was imaged by the FZP onto the sensor. The system was illuminated by an elongated laser beam (~5 W/cm^2) transformed by cylindrical lenses from a HeNe laser (wavelength = 633 nm, Melles Griot 25-LHP-928-249). The different components of the system are shown in Fig. 1(c)(d)(e).

Figure 1(c) shows the image of a PDMS microchannel attached to the aperture array. The microchannel was oriented at a small angle $\theta = 3.3^o$ with the aperture array. In the experiment, the channel spanned 44 apertures. In addition to the aperture array, an α-hole and a backup α-hole were drilled on the glass wafer with the same technique. The isolated α-hole had the same size as other apertures and was positioned at the center of the microchannel as shown in the figure. During the experiment, the α-hole and the corresponding β-hole (distance between them is 170 μm) in the aperture array downstream will scan the same part of the sample. By comparing the transmission from the α-hole and the β-hole, we can monitor the flow stability and measure the flow speed. The flow stability can be characterized by the correlation between time scan signals of the α, β-hole. Note that successful OFM imaging relies on the stability of sample flowing, so we must ensure that the sample does not rotate or change shape during the imaging process. The correlation of the transmissions through α, β-hole provides a good criteria for rejecting images of unstable samples. The flow speed V can be calculated by

$$V = \frac{d}{\tau} \tag{2}$$

where d and τ are the distance and the travel time of the sample between the α, β-hole, respectively. We further note that the rotation of spherical samples in the microfluidic flow can be significantly reduced through the use of electrokinetic actuation and this approach has been employed in other versions of the optofluidic microscope [2].

Figure 1(d) is a microscope image of the fabricated FZP. The FZP was a phase reversal FZP where the optical thickness of adjacent zones differed by half of the laser wavelength. Given the refractive index of SU-8, n = 1.596, the thickness of spin-coated SU-8 was set to be near

$$t = \frac{\lambda}{2(n-1)} = 531\,nm \tag{3}$$

The phase reversal FZP has improved diffraction efficiency for the principle focus and is especially suitable for monochromatic illumination [5]. Note that in our case, the error in diffraction efficiency will be less than 5% if the thickness error in spin coating is less than 50 nm [11], which is achievable with spin-coating.

To reduce stray light from transmitting through the peripheral of the FZP, we proceeded to coat the peripheral with a layer of aluminum. The process is as described here. First, the entire wafer (on the FZP side) was coated with a thin layer of aluminum (thickness = 300 nm). Next, a layer of SPR220 photoresist was spin-coated on this aluminum layer by the spinner WS-400A-6NPP/LITE (Laurell Technologies). The photoresist directly on top of the FZP was then removed by photolithography. Finally the aluminum covering the FZP was removed by aluminum etchant (Transene Company) and the remaining SPR220 was washed away with acetone.

The image of the aperture array projected by the FZP onto the optical sensor is shown in Fig. 1(e). We can see that the transmission of all apertures, except those blocked by the edges of the microchannel, were well projected and distinguishable from each other. Note that the detected optical power from different apertures varies and, as such, we need to normalize the power of the apertures during data processing.

#99006 - $15.00 USD Received 17 Jul 2008; revised 6 Sep 2008; accepted 11 Sep 2008; published 18 Sep 2008

Before the experiment, the surface of the channel was coated with Poly(ethylene glycol) (PEG) to promote smooth microfluidic flow [12]. During the experiment, the channel was oriented vertically to actuate microfluidic flow by gravity. Note that other techniques, such as electroosmosis flow [2] or optical tweezer [3], can also be used to drive the samples scanning in the OFM system and maybe more suitable for other specific applications. While the sample was flowing through the microfluidic channel, the transmitted light of the aperture array was detected by the imaging sensor and each aperture effectively acquired a line scan of the sample.

The principle of image reconstruction was similar as our previous OFM systems [1-3] and can be briefly described as follows. Each line of the reconstructed image is actually a time-shifted line scan from the corresponding aperture. The time shift between adjacent line scans Δt can be expressed as, using equation (2),

$$\Delta t = \frac{L\cos\theta}{V} = \frac{L}{d}\tau\cos\theta \tag{4}$$

where L is the separation between adjacent apertures. In the final OFM image, the pixel size in x-direction (δx) and in y-direction (δy) can be calculated as

$$\delta x = \frac{V}{F},\ \delta y = L\sin\theta \tag{5}$$

where F is the frame rate of the imaging sensor. Suppose the length of the sample is l, then the image acquisition time can be expressed as

$$T = \frac{jL\cos\theta + l}{V} = j\Delta t + \frac{l}{V} \tag{6}$$

where j is the total number of apertures that scan the sample.

To characterize the imaging quality of the FZP, we used a 1-μm pinhole as our object and recorded its image while translating it along x-direction, as shown in Fig. 2(a). We then measured the image spot sizes at full-width-half-maximum (FWHM) in both x and y-direction by fitting the spot with a Gaussian profile and plotted them against the x position of the object, as shown in Fig. 2(c). As expected, the spot size and the error of the fitting along x-direction increased as the pinhole moved away from the center and the imaging spot became larger and more irregular. In contrast, the spot diameter along y-direction remained approximately the same as there was no y-displacement of the pinhole. We also note that the spot size for on-axis pinhole was approximately 10 μm, corresponding to a resolution of 10/M = 2.5 μm in object space. This is in fair agreement with the theoretical resolution of ~2.4 μm, which can be calculated based on the diameter of the FZP. In Fig. 2(c), we also show the pinhole images at three different x positions. According to this experiment, we can see that there is a resolution limit for extended object if the FZP is used for direct imaging. To maintain the best resolution, the image can not be extended more than 100 μm away from the axis, corresponding to an object size of less than 100/M * 2 = 50 μm. With the image scheme of OFM, however, the aberration issue is not important as long as the image light spots associated with the transmissions from the apertures can be resolved and separated from each other. As shown in Fig. 2(b), in FZP direct imaging, we will need to resolve object points with a separation of the on-axis resolution of FZP to achieve the optimal resolution, and the corresponding imaging spot separation is 2.5*M = 10 μm. While in the FZP-OFM scheme, the FZP projection will only need to resolve adjacent apertures which usually have a larger separation (10 μm in our case) than the on-axis resolution of the FZP. Thus the FZP-OFM can accept an aberrated imaging spot size of the aperture image separation, and the corresponding imaging spot separation is 10*M = 40 μm. This resolution is needed to perform high-resolution OFM imaging, as indicated in Fig. 2(c). In this case, the imaging resolution is determined by the size of the aperture and the distance between the sample and the aperture

#99006 - $15.00 USD Received 17 Jul 2008; revised 6 Sep 2008; accepted 11 Sep 2008; published 18 Sep 2008

instead of the imaging quality of FZP. As such, it is still possible to achieve high resolution imaging for larger field of view. The extension of our effective aperture array is 440 μm, i.e., 220 μm away from the axis, and is well within the capability of our FZP-OFM system. As expected, the acquired OFM images shown in the next section is much better than the images acquired by direct FZP imaging.

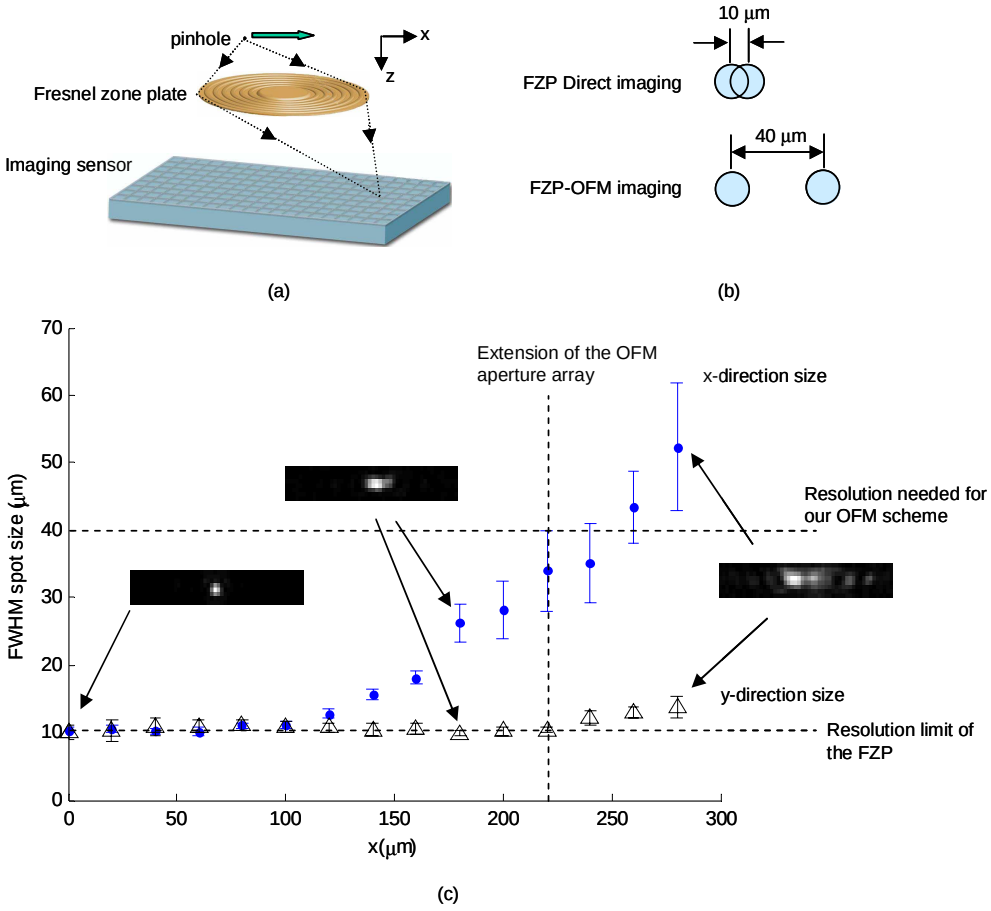

Fig. 2. (a) Experimental scheme to characterize the imaging quality of the FZP; (b) Demonstration of resolution needed to perform FZP direct imaging and FZP-OFM imaging; (c) Measured FWHM spot size of the image in x and y-direction versus the x position of a 1-μm pinhole. Pinhole images in three different positions are shown. The resolution limit of the FZP and the resolution needed for the FZP-OFM imaging are indicated.

3. Imaging results

As a demonstration, we acquired images of the protist *Euglena gracilis* (Carolina biology supply company) with the FZP-OFM system. We immobilized the protists by treating them in a 90°C heat bath for 15 second. The solution containing the protists was then injected into the input port of the FZP-OFM system. By tilting the FZP-OFM vertically, we were able to induce the solution to flow through the microfluidic channel. During the imaging process, the flow speed of the protists was measured by the α, β-hole pair to be $V \sim 400$ μm/sec. The imaging sensor was operated at a frame rate of $F = 1350$ frames/sec. The pixel spacing (or size) of the OFM images was $\delta x = 0.3$ μm and $\delta y = 0.6$ μm. The acquisition time for the protists images is ~1 sec. The resolution of the OFM system can be characterized by the point spread function (PSF) associated with the imaging aperture. We can achieve an optimal

#99006 - $15.00 USD Received 17 Jul 2008; revised 6 Sep 2008; accepted 11 Sep 2008; published 18 Sep 2008

resolution determined by the aperture size when the sample is very close to the aperture (in the optical near field regime). Since the width of the PSF increases as the height of the point object increases, the resolution of our OFM system will degrade with increasing distance between the sample and the aperture. The PSF can be measured by laterally scanning a near field scanning optical microscope (NSOM) tip across the aperture at different height H and measure the transmitted signals through it [13]. We measured the width of the PSF for the 1-μm aperture used in our experiment to be 0.9 μm when H = 0.1 μm and 3 μm when H = 2.5 μm. Thus the ultimate resolution of our OFM system is 0.9 μm.

Figure 3 is an image compilation of similar protists acquired with the FZP-OFM and other imaging schemes. Figure 3(a) was acquired by simply using a FZP to directly image a protist onto our optical sensor. We can see that the image is blurry and is negatively impacted by the presence of a diffraction background. In comparison, the FZP-OFM images shown in Fig. 3(b) are clearer and well-resolved. Since our FZP-OFM system used coherent laser as illumination, we believe that a comparison of the acquired images to those from a conventional microscope operating with coherent illumination and incoherent illumination would be helpful. Figure 3(c) and (d) show images of the protist that are acquired with a microscope (Olympus BX41) through a 20x objective under coherent and incoherent illumination, respectively.

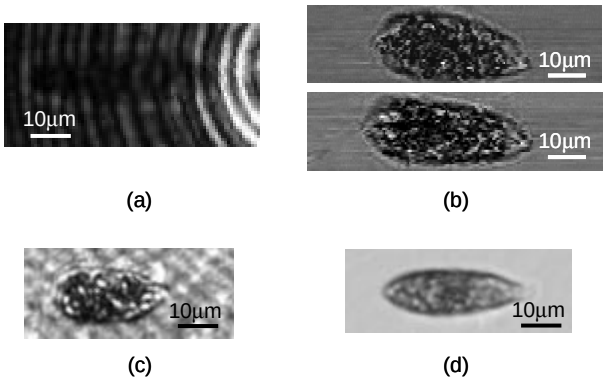

Fig. 3. Images of *Euglena gracilis* acquired by (a) FZP direct imaging; (b) FZP-OFM system; (c) Conventional microscope with 20x objective under coherent illumination; (d) Conventional microscope with 20x objective under incoherent illumination.

It is interesting to note that the FZP-OFM images appear to be more similar to the incoherent illumination conventional microscope image than the coherent illumination conventional microscope image, despite the fact that FZP-OFM also employed a coherent illumination source. The speckle background in Fig. 3(c) arose from the interference of stray light components scattered and reflected from various interfaces in the microscope. This pattern varied spatially but had no time varying component. The absence of this speckle background in Fig. 3(d) is attributable to the wash-out of such interference effect in incoherent illumination. The absence of the speckle background in our FZP-OFM images can be explained by noting that each horizontal line in the images represents a time trace of an aperture in the array. In the absence of an object directly above the aperture, we can expect the transmission through the aperture to remain unchanged in time. The transmission through each aperture was normalized with respect to each other at the beginning of the experiment. This was intended to correct for small variations in the aperture size and sensor sensitivity. However, variations in light intensity incident on the apertures would be, likewise, normalized by this process. As such, the impact of a speckle background in the FZP-OFM was effectively eliminated. We further note that the effect of mutual light interference from scatterings within the object should remain in our FZP-OFM images.

#99006 - $15.00 USD Received 17 Jul 2008; revised 6 Sep 2008; accepted 11 Sep 2008; published 18 Sep 2008

4. Summary

We have shown that the FZP can be incorporated into the OFM design to create a modified FZP-OFM scheme. We showed that the aberrations associated with FZP did not impact or limit the resolution of the FZP-OFM, which is limited fundamentally by the size of apertures employed. We further presented the use of our FZP-OFM prototype to acquire microscopy images of protists. The absence of a speckle background in our FZP-OFM images was an unexpected observation that can be explained by closely examining the OFM's imaging strategy.

As this scheme allows the separation of the OFM aperture array from the optical sensor array, it is advantageous for a number of scenarios. Specifically, this design allows for easier recycling of high-cost optical sensor array and it allows for the cooling of the optical sensor with less risk of freezing shut the microfluidic channel.

Acknowledgments

The authors would like to acknowledge Dr. Xin Heng for helpful discussions. This project is supported by the NSF career award BES-0547657.

#99006 - $15.00 USD Received 17 Jul 2008; revised 6 Sep 2008; accepted 11 Sep 2008; published 18 Sep 2008